

JGR Space Physics

RESEARCH ARTICLE

10.1029/2019JA027377

Key Points:

- A reference frame moving with respect to the solar wind plasma can often be found wherein the flow vector is everywhere parallel to the field vector
- This is the frame of the heliospheric magnetic structure moving outward through the solar wind plasma at ~0.7 times the Alfvén speed
- The degree of plasma homogeneity is hypothesized to control the motion of the structure relative to the plasma

Correspondence to:

J. E. Borovsky, jborovsky@spacescience.org

Citation:

Borovsky, J. E. (2020). On the motion of the heliospheric magnetic structure through the solar wind plasma. *Journal* of *Geophysical Research*: *Space Physics*, 125, e2019JA027377. https://doi.org/ 10.1029/2019JA027377

Received 6 SEP 2019 Accepted 25 OCT 2019 Accepted article online 17 JAN 2020

On the Motion of the Heliospheric Magnetic Structure Through the Solar Wind Plasma

Joseph E. Borovsky¹

¹Center for Space Plasma Physics, Space Science Institute, Boulder, CO, USA

Abstract A reference frame in the solar wind can often be found wherein the flow vector \underline{v} is everywhere approximately parallel to the magnetic field vector \underline{B} . This is the frame of the heliospheric magnetic structure moving relative to the plasma. Since v_{\perp} is very small in this reference frame, the magnetic structure appears to have little temporal evolution. The structure moves outward away from the Sun faster than the plasma flow. Even for highly Alfvénic plasma, the structure does not move at the Alfvén speed relative to the proton plasma, rather it moves at ~0.7 $v_{\rm A}$. This may be caused by the spread in the vector directions of the local magnetic field. The degree of inhomogeneity of the plasma is hypothesized to control the motion of the magnetic structure through the plasma. If so, non-Alfvénicity may be owed to an inability of Alfvénic perturbations to coherently propagate from Alfvénic injections at the Sun. Schemes that mathematically advect magnetic and plasma structure from upstream solar wind monitors to the Earth may be improved by calculating and including the motion of the structure relative to the solar wind velocity vector.

1. Introduction

Solar wind measurements are characterized by fluctuations at all timescales. For timescales longer than 1 s or so, it can be safely assumed that the temporal fluctuation at a spacecraft is owed to spatial fluctuations in the solar wind structure that is advected past the spacecraft. Often the fluctuations are Alfvénic, with strong temporal correlations between the flow vector $\underline{v}(t)$ and the magnetic-field vector $\underline{B}(t)$. Examinations of the time series of measurements find a dominance of current sheets in the magnetic field measurements and of velocity shears in the flow measurements (Borovsky, 2012a; Bruno, 2019; Siscoe et al., 1968; Veltri & Mangeney, 1999). Interpretation of these current sheets and velocity shears has focused on MHD (magnetohdrodynamic) turbulence, coronal flux tubes, mirror modes, pressure-balance structure, and reconnection outflows. There are outstanding questions about the nature and origin of the structure of the solar wind, a particularly interesting one is what parts of the structure are relics from the Sun and what parts of the structure are created and recreated in situ in the solar wind plasma (Li & Qin, 2011; Neugebauer & Giacalone, 2010, 2015; Owens et al., 2011; Tu et al., 2016).

The magnetic structure of the solar wind is of interest for a number of reasons. The magnetic structure acts to duct energetic particles (McCracken & Ness, 1966; Tessein et al., 2016; Trenchi et al., 2013) and to scatter energetic particles (Qin & Li, 2008; Zimbardo et al., 2008), understanding particle transport and interpreting particle measurements requires some understanding of the properties of the heliospheric magnetic structure. The propagation of interplanetary shocks (Chashei & Shishov, 1995; Heinemann & Siscoe, 1974; Zank et al., 2003) and the acceleration of particles by shocks is dependent on the nature of the magnetic structure (Guo & Giacalone, 2010; Kocharov et al., 2013; Niemiec & Ostrowski, 2004; Sandroos & Vainio, 2006); an understanding of the properties of the heliospheric magnetic structure is needed to understand these shock processes. The nature of the solar wind plasma and magnetic structure also can be important for the propagation of coronal mass ejections through the heliosphere (Borovsky, 2006; Lavraud et al., 2014; Schwenn, 2000; van der Holst et al., 2005; Zhou & Feng, 2017). The details of the magnetic structure of the solar wind at Earth are of great interest to magnetospheric physics and space weather forecasting (Borovsky, 2018a; Morley et al., 2018; Walsh et al., 2019; Weimer & King, 2008): the rate of reconnection between the solar wind and the magnetosphere controls the strength of the driving of the magnetosphere and that reconnection rate depends critically on the orientation of the solar wind magnetic field vector at Earth (Komar et al., 2015; Liu et al., 2015; Sonnerup, 1974).

©2020. American Geophysical Union. All Rights Reserved.

BOROVSKY 1 of 14



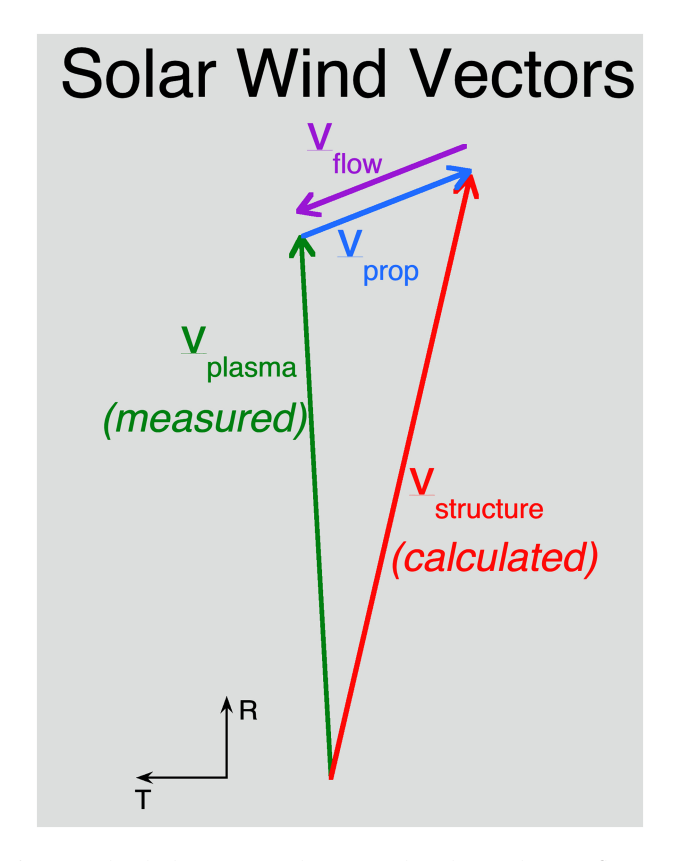


Figure 1. Sketched in RTN coordinates are the solar wind proton flow vector as measured by the spacecraft (green), the reference frame of the magnetic structure calculated with the evolutionary algorithm (red), and the motion (propagation) of the structure through the plasma (blue). Also shown (purple) is the flow vector of the plasma through the magnetic structure as seen by the magnetic structure.

The magnetic structure also delineates a plasma structure, with sudden changes in number density, plasma beta, proton specific entropy, electron heat flux, and helium abundance occurring across the current sheets of the solar wind (Borovsky, 2008; Borovsky, 2020; Khabarova & Zastenker, 2011; Riazantseva et al., 2005; Tu et al., 2016). There is also a velocity structure associated with the magnetic structure (De Keyser et al., 1998; Denskat & Burlaga, 1977; Neugebauer, 1985), which will be explored in the present study. The Earth's magnetotail can be disrupted by the strong velocity shears in the solar wind associated with magnetic current sheets (Borovsky, 2012a, 2018b).

Advancing our understanding of the properties of the heliospheric magnetic structure can provide help for the abovementioned problems of space research. Advancing our understanding of the properties of the structure might also lead to clues about the origin of the structure, to clues about the evolution (or not) of the structure and perhaps to clues about the origin of the solar wind.

In this report we point out that there often is a frame of reference in which the proton flows of the solar wind plasma are everywhere parallel to the local magnetic field. It will be argued that this reference frame moves with the tangled magnetic structure, which moves through the solar wind proton plasma. The relevant solar wind vectors describing this are sketched in Figure 1. In this reference frame, the changing velocity of the solar wind appears as a field-aligned flow through the magnetic structure, with the flow changing direction spatially as the field changes direction spatially. Using 3-s measurements of the magnetic field and plasma at the WIND spacecraft, this frame will be explored. When this frame can be found, it appears that there is little ongoing evolution of the magnetic structure. This is equivalent to the De Hoffman-Teller reference frame of the solar wind that Nemecek et al. (2020) use to analyze the kinetic distribution functions of solar wind protons, alpha particles, and heavy ions.

This manuscript is organized as follows. In section 2 the data sets and methodologies used are explored. In section 3 examples in three types of wind are examined, in section 3.1 unperturbed coronal-hole-origin plasma, in section 3.2 Alfvénic slow wind, and in section 3.3 non-Alfvénic slow wind. Section 4 contains discussions about the nature of the solar wind structure (section 4.1), the Alfvénicity, inhomogeneity, and compressibility of the solar wind (section 4.2), the speed of the structure relative to the plasma (section 4.3), turbulence scaling estimates (section 4.4), and solar wind propagation schemes for Earth (section 4.5).

2. Data and Methods

The 3-s resolution magnetic field measurements $\underline{B}(t)$ from WIND Magnetic Field Investigation (Lepping et al., 1995) and 3-s resolution plasma and flow measurements $\underline{v}_{plasma}(t)$ from WIND 3DP (three-dimensional plasma) (Lin et al., 1995) are used to study the motion of the mesoscale magnetic-field structure of the heliosphere moving through the proton plasma of the solar wind. If a reference frame with velocity $\underline{v}_{structure}$ can be found wherein ($\underline{v}_{plasma} - \underline{v}_{structure}$) $\times \underline{B} = 0$ consistently, then this frame is consistent with the reference frame of the magnetic structure wherein all flows seen in that frame are locally parallel to the local magnetic field.

Data subintervals that are either 30, 60, 120, or 180 min long are analyzed. Times when there is bad plasma or bad magnetic field measurements are removed from the analysis. (This removal includes plasma measurements in the 3DP data set wherein $v_x \equiv 0.00$, $v_y \equiv 0.00$, or $v_z \equiv 0.00$.) The magnetic field measurement closest to the time of each plasma measurement is used in conjunction with the flow velocity: data values wherein the time between plasma and field measurements is greater than 6 s are removed.

BOROVSKY 2 of 14

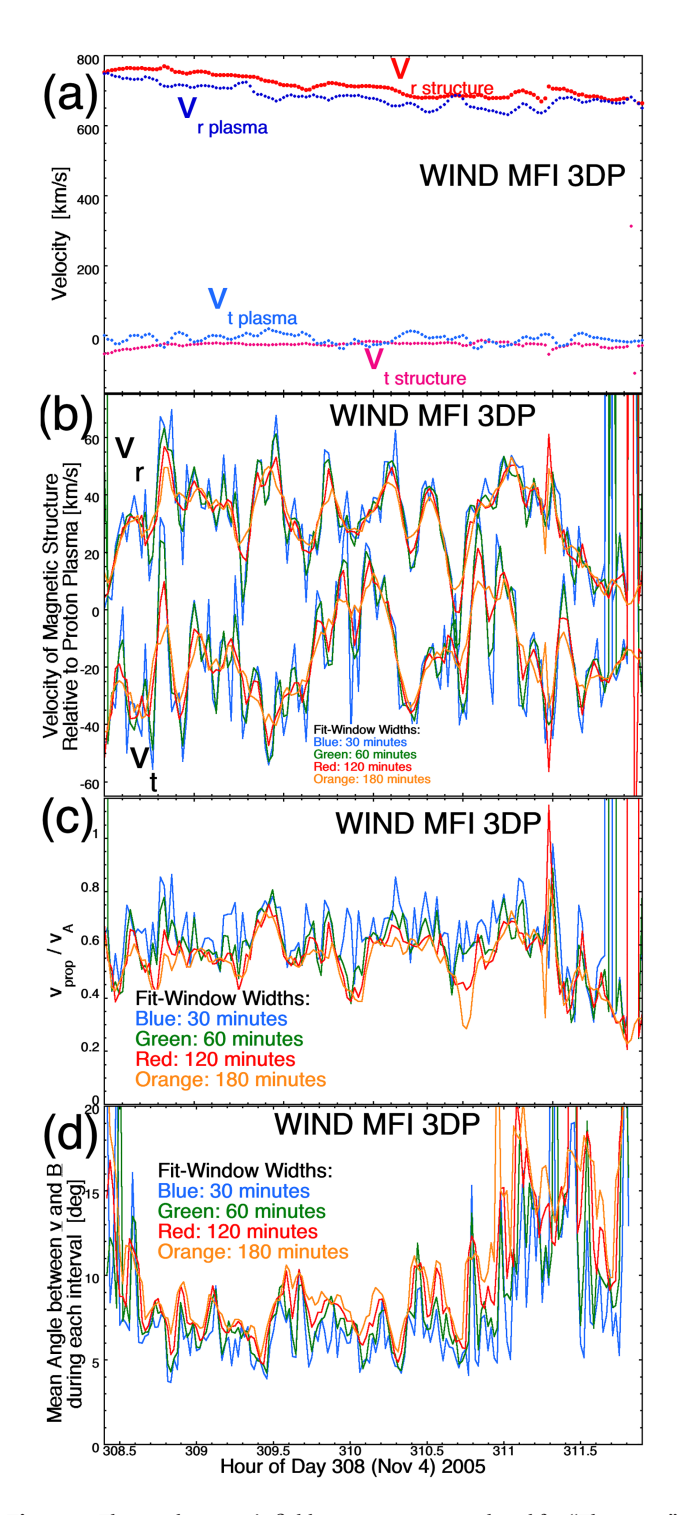


Figure 2. Flow and magnetic field measurements analyzed for "Flattop 15" of Borovsky (2016a). In panel (a) the plasma flow and magnetic structure frame are plotted in the reference frame of the spacecraft. In panel (b) the velocity of the magnetic structure is plotted as seen from the rest frame of the proton plasma. In panel (c) the speed of the structure (relative to the proton plasma) divided by the Alfvén speed is plotted. In panel (d) the mean angle between the flow and the magnetic field in the frame of reference of the magnetic structure is plotted. In panels (b) and (c) the different colors are for different time widths of the data subintervals analyzed.

For each data subinterval a single reference frame $\underline{v}_{structure} = (v_{xstructure}, v_{ystructure}, v_{ystructure})$ is guessed. Then, using an iterative evolutionary algorithm $v_{xstructure}$, $v_{ystructure}$, or $v_{zstructure}$ is changed at each iteration by adding a random scalar -1 km/s $< \Delta v < +1$ km/s. Denoting the WIND 3DP measured proton flow vector as \underline{v}_{plasma} , the angles arccos $(\underline{v}_{flow} \bullet \underline{B})$ between $\underline{v}_{flow} \equiv (\underline{v}_{plasma} - \underline{v}_{structure})$ and \underline{B} are calculated for each 3-s data point in the subinterval, and the average value of that angle is calculated for the subinterval. If the average value of the angle is reduced by the change, then the change to $\underline{v}_{structure}$ is kept; if the average value of the angle is not reduced by the change, the change is rejected. In this manner, $\underline{v}_{structure}$ evolves to a vector value that minimizes the average angle between $(\underline{v}_{plasma} - \underline{v}_{structure})$ and \underline{B} for the subinterval. Typically, a minimum value of the angle (and a value for $\underline{v}_{structure}$) is reached in about 2,000 iterations.

3. The Movement of the Magnetic Structure

The movement of the heliospheric magnetic structure through the solar wind plasma will be examined for three examples: unperturbed coronal-hole-origin plasma in section 3.1, Alfvénic slow wind in section 3.2, and non-Alfvénic slow wind in section 3.3.

3.1. Unperturbed Coronal-Hole-Origin Plasma

In Borovsky (2016a) a number of intervals of unperturbed coronal-holeorigin plasma were identified at 1 AU, where "unperturbed" means the high-speed stream plasma was not in a compression region (corotating interaction region) or in a rarefaction region (trailing edge of a high-speed stream). WIND Magnetic Field Investigation and 3DP measurement for "Flattop 15" (cf. Table 1 of Borovsky, 2016a) is explored. At the first Lagrangian Point L1 upstream of the Earth, Flattop 15 commenced at 13 UT on Day 308 (4 November) of 2005 and ended at 12 UT on Day 311 (7 November). In Figure 2a data subintervals every 30 min are analyzed; each subinterval is 120 min wide. For each data subinterval the evolutionary algorithm is used to derive a frame shift v_{structure} that minimizes the average of the 3-s values in the subinterval of the angle between $(\underline{v}_{plasma}(t) - \underline{v}_{structure})$ and $\underline{B}(t)$. In Figure 2a the average velocity of the plasma \underline{v}_{plasma} for each subinterval is plotted in blue, and the calculated value of the velocity of the magnetic structure v_{structure} (cf. Figure 1) for each subinterval is plotted in red. The upper curves are the R (radial) component of the velocities and the lower curves and the T (tangential) components. The N (normal) components of the plasma and structure velocities are not plotted. As can be seen, the magnetic structure (red and pink) tends to move away from the Sun faster than the proton plasma and moves faster in the negative tangential direction: This is consistent with the structure propagating outward in the Parker-spiral direction through the solar wind plasma. In Figure 2b the velocity of the magnetic structure relative to the proton plasma ($v_{structure} - v_{plasma}$) is plotted. The

BOROVSKY 3 of 14

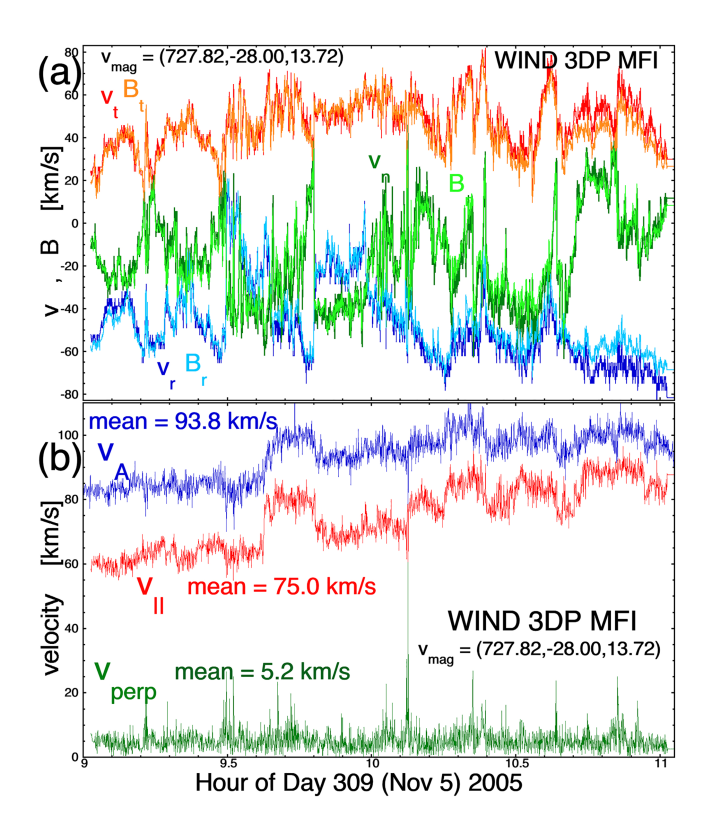


Figure 3. An example from Flattop 15 using 2 hr of measurements to calculate a velocity (727.82,—28.00,13.71) km/s for the magnetic structure. In panel (a) the 3-s flow and (normalized) magnetic field measurements are plotted in the reference frame moving with the magnetic structure. In panel (b) the 3-s flow measurements are decomposed in parallel and perpendicular components using the 3-s measurements of the magnetic field direction.

lower curves are the tangential component of the structure velocity, and the upper curves are the radial component. The four different colors in Figure 2b are for four different data-interval widths: 30 min (blue), 60 min (green), 120 min (red), and 180 min (orange). The radial component of the velocity of the magnetic structure tends to be positive, with the structure moving out away from the Sun faster than the solar wind proton plasma. The tangential component of the velocity of the magnetic structure tends to be negative, consistent with the structure moving outward along the Parker-spiral direction through the plasma. In Figure 2c the speed of the structure relative to the plasma $v_{prop} = |\underline{v}_{structure} - \underline{v}_{plasma}|$ is plotted divided by the average of the Alfvén speed in each subinterval. The Alfvén speed is calculated from 3DP 3-s measurements of the proton number density n_p , with $n_{\alpha}/n_p = 0.045$ used; the onboard 3DP 3-s moments do not calculate the alpha-particle density accurately for high-speed wind, so the average value of n_{α}/n_{p} for Flattop 15 from WIND Solar Wind Experiment (Kasper et al., 2006) was used. As can be seen in Figure 2c, the speed of the magnetic structure moving through the solar wind plasma tends to be less than the Alfvén speed. In Figure 2d the average of the 3-s resolution angles $arccos (\underline{v}_{flow} \cdot \underline{B})$ between $\underline{\mathbf{v}}_{flow} = (\underline{\mathbf{v}}_{plasma}(t) - \underline{\mathbf{v}}_{structure})$ and $\underline{\mathbf{B}}(t)$ is plotted, with the average over 30-min (blue), 60-min (green), 120-min (red), or 180-min (orange) subintervals in different colors. As can be seen, in favorable subintervals the mean angle between the flow and the field can be $\sim 5^{\circ}$.

For one 2-hr-long data subinterval in the unperturbed-coronal-hole plasma of Flattop 15, the 3-s measurements of the flow and magnetic field from the reference frame of the moving magnetic structure are examined in Figure 3. The subinterval is chosen for its low value of the mean angle between the flow and the field; that is, it is an example of a time when a reference frame describing moving structure is found. The average parameters for this 2-hr subinterval are solar wind flow speed $v_{\rm sw} = \langle |v_{\rm plasma}| \rangle$

= 672 \pm 42 km/s, magnetic field strength $B_{\rm mag}$ = 4.6 \pm 1.1 nT, and proton number density n_p = 1.7 \pm 0.8 cm⁻³. For the 2-hr subinterval, the derived frame shift is $\underline{v}_{\text{structure}} = (727.82, -28.00, -13.72) \text{ km/s in RTN}$ coordinates. For this 2-hr subinterval, the average 3-s angle between $(\underline{v}_{plasma} - \underline{v}_{structure})$ and \underline{B} in the reference of the subinterval of the sub ence frame of the magnetic structure is 4.8°; the average spread of angles of the direction of B around the mean field direction is $20.8 \pm 11.2^{\circ}$ in the 2-hr subinterval. In Figure 3a the three velocity components v_{rplasma} - v_{rstructure} (dark blue), v_{tplasma} - v_{tstructure} (red), and v_{nplasma} - v_{nstructure} (dark green) are plotted as functions of time and the three normalized components of the magnetic field B_r (light blue), B_t (orange), and B_n (light green) are plotted. The normalization of the magnetic field is a multiplication by a single scalar value $v_{\mathrm{flow}}/B_{\mathrm{mag}}$, where $v_{\mathrm{flow}} = \langle |\underline{v}_{\mathrm{plasma}} - \underline{v}_{\mathrm{structure}}| \rangle$ is the average of the plasma flow in the reference frame of the magnetic structure and $B_{\text{mag}} = \langle |\underline{B}| \rangle$ is the average of the magnetic field strength, with the averaging $\langle \ \rangle$ over the entire 2-hr subinterval. As can be seen, for much of the subinterval the components of the vector $\underline{v}_{plasma} - \underline{v}_{structure}$ are indistinguishable from the components of the normalized magnetic field vector B. In Figure 3b the vector $\underline{\mathbf{v}}_{plasma} - \underline{\mathbf{v}}_{structure}$ is decomposed every 3 s into its parallel-to- $\underline{\mathbf{B}}$ (red) and perpendicularto-B (green) components v_{\parallel} and v_{\perp} . For this 2-hr subinterval the mean value of v_{\parallel} is 75.0 km/s and the mean value of v_{\perp} is 5.2 km/s. In this magnetic-structure reference frame, v_{\parallel} is on average more than 14 times v_{\perp} . Some of the v_{\perp} can be attributed to measurement inaccuracy of the flow vector and measurement inaccuracy of the magnetic field direction. A large source of the v_{\perp} comes from the fact that the magnetic field direction changes during the 3-s measurement of the flow. For the 2-hr interval of Figure 3 the mean and standard deviation of the 3-s angular change in the magnetic field direction is $\Delta\theta_{3-s} = 4.5 \pm 4.4^{\circ}$: taking $\nu_{||} \sin{(\Delta\theta_{3-s})}$ with $\Delta\theta_{3-s} = 4.5^{\circ}$ and with $\nu_{\parallel} = 75.0$ km/s yields 5.9 km/s as an estimate of the amount of ν_{\perp} coming from a pro $jection\ of\ v_{||} attributable\ to\ the\ motion\ of\ the\ field\ direction.\ Also\ plotted\ (blue)\ in\ Figure\ 3b\ is\ the\ 3-s\ value\ of\ plotted\ (blue)\ in\ Figure\ 3b\ is\ the\ 3-s\ value\ of\ plotted\ (blue)\ in\ Figure\ 3b\ is\ the\ 3-s\ value\ of\ plotted\ (blue)\ in\ Figure\ 3b\ is\ the\ 3-s\ value\ of\ plotted\ (blue)\ in\ Figure\ 3b\ is\ the\ 3-s\ value\ of\ plotted\ (blue)\ in\ Figure\ 3b\ is\ the\ 3-s\ value\ of\ plotted\ (blue)\ in\ Figure\ 3b\ is\ the\ 3-s\ value\ of\ plotted\ (blue)\ in\ Figure\ 3b\ is\ the\ 3-s\ value\ of\ plotted\ (blue)\ in\ Figure\ 3b\ is\ the\ 3-s\ value\ of\ plotted\ (blue)\ in\ plotted\$ v_A , with a mean value and standard deviation of 73.9 \pm 11.9 km/s in the 2-hr subinterval. As seen, the flows

BOROVSKY 4 of 14

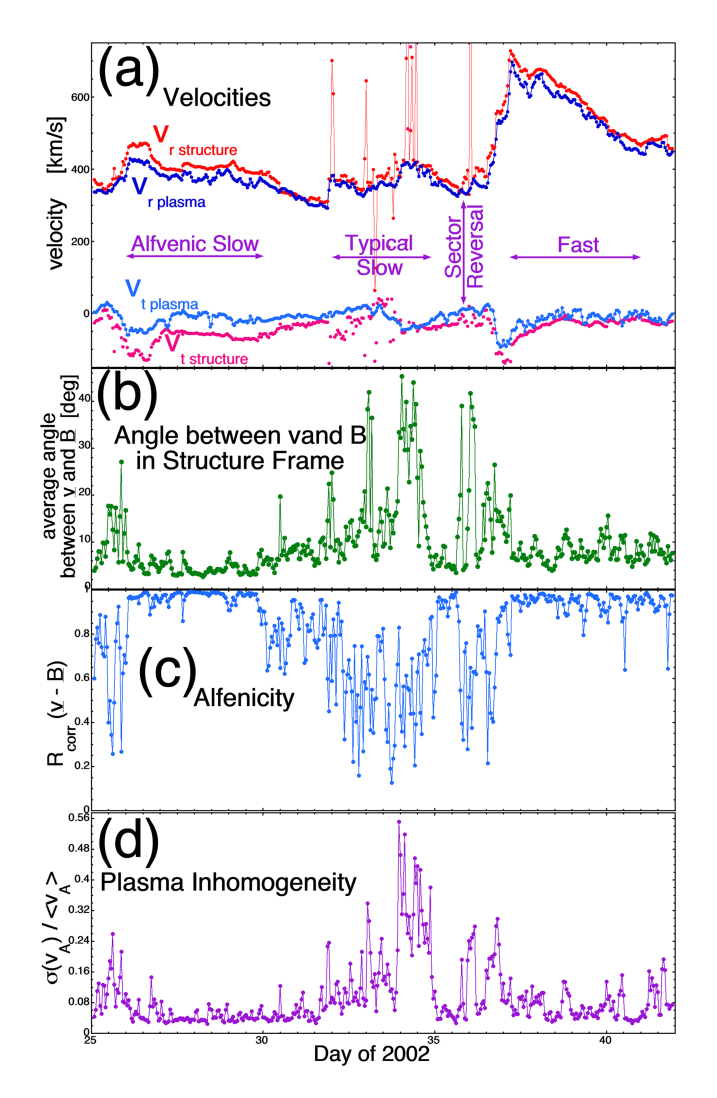


Figure 4. The interval of Figures 1 and 3 of D'Amicis et al. (2019) is analyzed using 120-min data subintervals. In panel (a) the measured plasma velocity and the calculated magnetic structure velocity is plotted. In panel (b) the mean angle in each data subinterval between the 3-s flow vector and the 3-s magnetic field vector. In panel (c) the Alfvénicity (*v-B* correlation coefficient) is plotted for each 120-min subinterval. In panel (d) the inhomogeneity of the plasma as measured by the standard deviations of the 3-s Alfvén speeds divided by the mean value of the Alfvén speeds.

of plasma through the magnetic structure (in the structure's reference frame) are at a fraction of the Alfvén speed.

3.2. Alfvénic Slow Wind

There has been recent interest in the fact that nonejecta slow solar wind can be either Alfvénic or not (Borovsky et al., 2019; D'Amicis et al., 2016, 2019; D'Amicis & Bruno, 2015). In the Xu and Borovsky (2015) categorization scheme for solar wind plasma, Borovsky et al. (2019) attribute the Alfvénic slow wind to plasma originating from the streamer belt and the non-Alfvénic slow wind to plasma originating from the sector reversal region around the heliospheric current sheet.

In Figure 4, the 17-day interval plotted in Figures 1 and 3 of D'Amicis et al. (2019) is plotted. Using 120-min subintervals of the 3-s WIND data, the structure velocity for each subinterval is calculated with the evolutionary algorithm and the radial (red) and tangential (pink) components of the velocity of the magnetic structure v_{structure} (cf. Figure 1) are plotted in Figure 4a. The average value of the measured plasma flow for each 120min subinterval is also plotted, the radial component in dark blue, and the tangential component in light blue. The intervals identified by D'Amicis et al. (2019) as Alfvénic slow wind, typical slow wind, and fast wind are labeled with the horizontal purple arrows in Figure 4a. The time of occurrence of a magnetic sector reversal is labeled with the vertical purple arrow. In Figure 4b the average of the 3-s angles arccos ($v_{flow} \cdot B$) between the flow velocity $v_{\rm flow}$ (cf. Figure 1) as seen from the reference frame of the magnetic structure $\underline{v}_{flow} = (\underline{v}_{plasma} - \underline{v}_{structure})$ and the magnetic field vector B is plotted. In Figure 4c the Alfvénicity of each 2-hr subinterval is plotted, with 1 being fully Alfvénic and 0 being non-Alfvénic. Here the Alfvénicity is measured by the absolute values of the Pearson linear correlation coefficients R_{corr} between v and B calculated as

$$R_{\text{corr}} = (|R_{\text{corr r}}| + |R_{\text{corr t}}| + |R_{\text{corr n}}|)/3 \tag{1}$$

where $R_{\rm corr\ r}$ is the correlation between $v_{\rm r}$ and $B_{\rm r}$, $R_{\rm corr\ t}$ is the correlation between $v_{\rm t}$ and $B_{\rm t}$, and $R_{\rm corr\ n}$ is the correlation between $v_{\rm n}$ and $B_{\rm n}$. In Figure 4d the inhomogeneity of the plasma in each 2-hr subinterval is plotted, as measured by the standard deviation of the 3-s values of $v_{\rm A}$ divided by the mean of the values.

Of interest for this subsection is the "Alfvénic slow" interval in Figure 4a. Note that for this interval the values of the angle between the flow and the field (green points) are low, often less than 5°. During this Alfvénic-solar-wind interval the magnetic structure (red and pink) clearly moves out

along the Parker spiral direction ahead of the solar wind proton plasma (dark and light blue).

In Figure 5 the 3-s flow and magnetic field data are examined for one 2-hr subinterval of Alfvénic slow wind from Figure 4. The subinterval is chosen for its low value of the mean angle between the flow and the field; that is, it is an example of a time when a reference frame describing moving structure is found. The average parameters for this 2-hr subinterval are $v_{\rm sw} = \langle |\underline{v}_{\rm plasma}| \rangle = 424 \pm 20$ km/s, $B_{\rm mag} = 9.4 \pm 0.1$ nT, and $n_p = 3.3 \pm 0.2$ cm⁻³. The frame shift for the magnetic structure derived by the evolutionary algorithm for this 2-hr subinterval is $\underline{v}_{\rm structure} = (472.26, -115.53, 0.30)$ km/s in RTN coordinates. For this 2-hr subinterval, the average 3-s angle between ($\underline{v}_{\rm plasma} - \underline{v}_{\rm structure}$) and \underline{B} in the reference frame of the magnetic structure is 4.8°; in the 2-hr subinterval the average spread of angles of \underline{B} around the mean-field direction is 24.1 \pm 11.8°. In Figure 5a the three velocity components $v_{\rm rplasma} - v_{\rm rstructure}$ (dark blue), $v_{\rm tplasma} - v_{\rm tstructure}$ (red), and $v_{\rm nplasma} - v_{\rm nstructure}$ (dark green) are plotted as functions of time and the three normalized components of the magnetic field $B_{\rm r}$ (light blue), $B_{\rm t}$ (orange), and $B_{\rm r}$ (light green) are plotted. The normalization

BOROVSKY 5 of 14

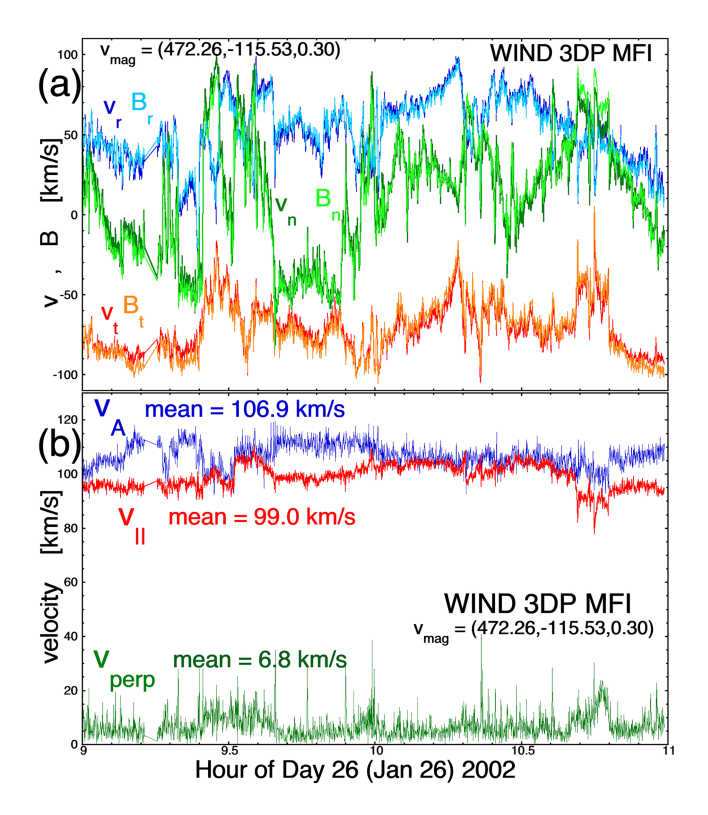


Figure 5. An example of Alfvénic slow wind using 2 hr of measurements from the D'Amicis et al. (2019) interval to calculate a velocity (472.26, -115.53,0.30) km/s for the magnetic structure. In panel (a) the 3-s flow and (normalized) magnetic field measurements are plotted in the reference frame moving with the magnetic structure. In panel (b) the 3-s flow measurements are decomposed in parallel and perpendicular components using the 3-s measurements of the magnetic field direction.

of the magnetic field is a multiplication by a single scalar value $v_{\text{flow}}/B_{\text{mag}}$, where $v_{\text{flow}} = \langle |v_{\text{plasma}} - v_{\text{structure}}| \rangle$ is the subinterval average of the plasma flow in the reference frame of the magnetic structure and B_{mag} $=\langle |B| \rangle$ is the subinterval average of the magnetic field strength. As was the case for the unperturbed-coronal-hole subinterval of Figure 3a, the velocity and magnetic curves in Figure 5a are almost undistinguishable: the flow vector points in the direction of the field vector. In Figure 5b the vector $\underline{\mathbf{v}}_{\text{plasma}} - \underline{\mathbf{v}}_{\text{structure}}$ is decomposed every 3 s into its parallel-to-B (red) and perpendicular-to-B (green) components v_{\parallel} and v_{\perp} using the 3-s values of the magnetic field direction. For this 2-hr subinterval the mean value of v_{\parallel} is 99.0 km/s and the mean value of v_{\parallel} is 6.8 km/s. In the reference frame moving with the magnetic structure, v_{\parallel} is on average more than 14 times v_{\perp} . Again, some fraction of the magnitude of v_{\perp} can be attributed (1) to measurement inaccuracy of the flow vector, (2) to measurement inaccuracy of the field direction, and in particular (3) to the variation of the direction of the magnetic field during the 3-s flow measurement. Also plotted (blue) in Figure 5b is the 3-s value of the Alfvén speed v_A using the 3DP values of n_p and n_α , with v_A having a mean value and standard deviation of $106.9 \pm 4.4 \text{ km/s}$ in the 2-hr subinterval; the flows of plasma through the magnetic structure (in the structure's reference frame) is at a large fraction of the Alfvén speed.

3.3. Non-Alfvénic Slow Wind

Of interest in this subsection is the interval in Figure 4a labeled "typical slow." Note that for this interval the values of the angle between the flow and the field (green points in Figure 4b) are larger than the prior intervals examined, varying from 4° to 45° in the various 2-hr subintervals. In Figure 4 the calculated frame for the magnetic structure (red and pink) clearly sometimes moves out along the Parker spiral direction ahead of the solar wind proton plasma (dark and light blue), but often, the value for the frame shift is erratic.

In Figure 6 the 3-s flow and magnetic field data are examined for one 2-hr subinterval of non-Alfvénic slow wind. This subinterval is chosen because it does not have a low value of the mean angle between the flow and the field; that is, it is an example of a time when a reference frame describing moving structure is not found. The average parameters for this 2-hr subinterval are $v_{\rm sw} = \langle |v_{\rm plasma}| \rangle = 390 \pm 14$ km/s, $B_{\rm mag} = 4.2$ \pm 0.9 nT, and $n_p = 6.9 \pm 1.2$ cm⁻³. The frame shift for the magnetic structure derived by the evolutionary algorithm for this 2-hr subinterval is $v_{structure} = (472.26, -115.53, 0.30)$ km/s. For this 2-hr subinterval, the average 3-s angle $\arccos{(\underline{v}_{flow} \bullet \underline{B})}$ between $\underline{v}_{flow} = (\underline{v}_{plasma} - \underline{v}_{structure})$ and \underline{B} in the reference frame of the magnetic structure is 18.5° ; in the 2-hr subinterval the average spread of angles of \underline{B} around the mean-field direction is 23.2 \pm 19.2°. In Figure 6a the three velocity components $v_{\rm rplasma} - v_{\rm rstructure}$ (dark blue), $v_{tplasma} - v_{tstructure}$ (red), and $v_{nplasma} - v_{nstructure}$ (dark green) are plotted as functions of time and the three normalized components of the magnetic field B_r (light blue), B_t (orange), and B_n (light green) are plotted. The normalization of the magnetic field is a multiplication by a single scalar value $v_{\rm flow}/B_{\rm mag}$ where $v_{flow} = \langle |\underline{v}_{plasma} - \underline{v}_{structure}| \rangle$ is the average of the plasma flow in the reference frame of the magnetic structure and $B_{\text{mag}} = \langle |\underline{\mathbf{B}}| \rangle$ is the average of the magnetic field strength. Contrary to the cases for the unperturbed-coronal-hole subinterval of Figure 3a and the Alfvénic-slow-wind subinterval of Figure 5a, the velocity and magnetic curves in Figure 6a for the non-Alfvénic slow wind subinterval are substantially different. In Figure 6b the vector $\underline{v}_{plasma} - \underline{v}_{structure}$ is decomposed every 3 s into its parallel-to-B (red) and perpendicular-to-B (blue) components v_{\parallel} and v_{\perp} . For this 2-hr subinterval the mean value of v_{\parallel} is 26.1 km/s, and the mean value of v_{\perp} is 4.5 km/s. In the reference frame moving with the magnetic structure, v_{\parallel} is on average more than 5 times v_{\perp} . This v_{\parallel}/v_{\perp} ratio is large, but not nearly as large as it is in the unperturbed coronal-hole-origin subinterval of Figure 3b or the Alfvénic-slow-wind subinterval of Figure 5b. Again, some of the v_{\perp} can be attributed to measurement inaccuracy of the flow and measurement

BOROVSKY 6 of 14

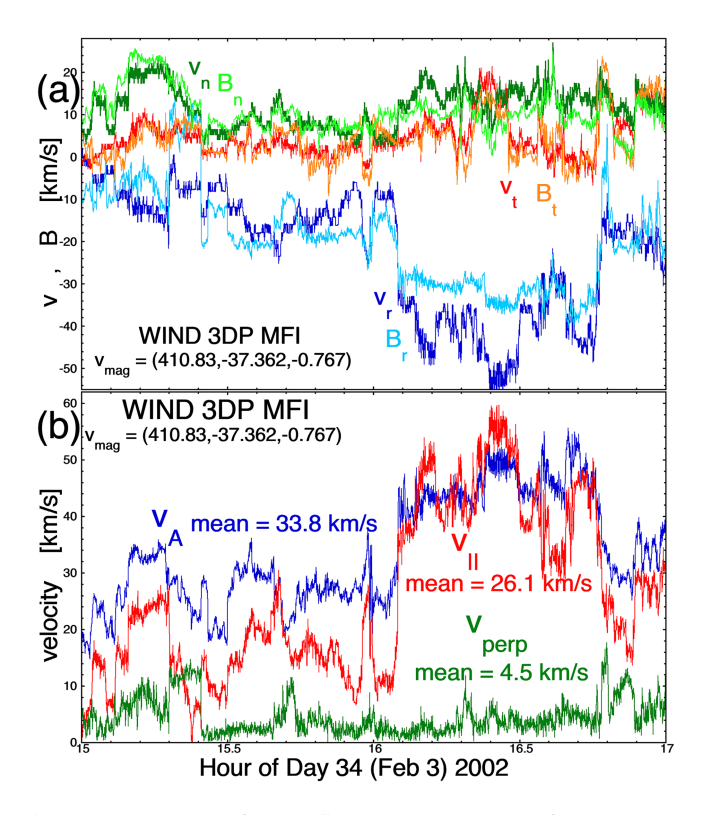


Figure 6. An example of "typical" slow wind using 2 hr of measurements from the D'Amicis et al. (2019) interval to calculate a velocity (410.83, -37.3623, -0.767) km/s for the magnetic structure. In panel (a) the 3-s flow and (normalized) magnetic field measurements are plotted in the reference frame moving with the magnetic structure. In panel (b) the 3-s flow measurements are decomposed in parallel and perpendicular components using the 3-s measurements of the magnetic field direction.

inaccuracy of the field direction. Also plotted (blue) in Figure 6b is the 3-s value of ν_A ; the flows of plasma through the magnetic structure (in the structure's reference frame) are at a fraction of the Alfvén speed or even exceeding the Alfvén speed. Note, however, that the evolutionary algorithm has not found a frame wherein the angle between the flow and the field is very small. Note in Figure 6b that the Alfvén speed varies substantially during this 2-hr subinterval, with the mean and standard deviation being 33.8 \pm 9.6 km/s.

4. Discussion

4.1. The Nature of the Structure

Using the evolutionary algorithm, frames of reference could be found wherein the flow of the proton plasma is everywhere approximately parallel to the magnetic field of the heliospheric structure, even though the spread in angles of the magnetic field direction is substantial. It is interpreted that this frame of reference moves with the magnetic structure, which moves relative to the solar wind plasma. In this reference frame of the structure, one sees the proton plasma flowing though the structure with v parallel to B everywhere. The temporal changes in B(t) that one sees on a spacecraft are owed to spatial variations B(r,t,n) that are advected past the spacecraft at the speed of the magnetic structure: Likewise, the temporal changes in the plasma flow v(t) that one sees on a spacecraft are owed to spatial changes v(r,t,n) of the flow within the magnetic structure that are also advected past the spacecraft at the speed of the magnetic structure. Changes in the density, specific entropy, plasma beta, helium abundance, and electron heat flux, which all correspond to the magnetic structure, are also advected past the spacecraft at the speed of the magnetic structure rather than at the speed of the solar wind plasma.

The lack of perpendicular flow v_{\perp} in the reference frame of the magnetic structure indicates that the magnetic structure is evolving only very

slowly, or not at all, as it moves outward. The reader is reminded that the ν_{\perp} values obtained in this study are certainly overestimates owing to the motion of the magnetic field direction during the 3-s plasma flow measurements.

4.2. Inhomogeneity-Alfvénicity-Compressibility

Sometimes a reference frame can be found wherein the angles between \underline{v} and \underline{B} are small, and sometimes such a frame cannot be found. Alfvénic intervals seem to have this reference frame and non-Alfvénic intervals do not. This can be seen by comparing Figures 4b and 4c. For the 120-min subintervals of Days 25–41 of 2002, the average angle between \underline{v}_{flow} (in the reference frame of the structure) and \underline{B} for each subinterval is plotted in Figure 7a as a function of the \underline{v} - \underline{B} correlation $R_{corr}(\underline{v}$ - $\underline{B})$ (cf. expression (1)). The mean of the angles is smaller when the correlation is larger, with a correlation coefficient between the mean angle and $R_{corr}(\underline{v}$ - $\underline{B})$ of -0.61. An argument is made here that the homogeneity of the plasma may also be important, particularly the spatial constancy of the Alfvén speed in the plasma. Envisioning a tangled-flux-tube structure (e.g., the "spaghetti" magnetic structure of Mariani et al., 1983), if the Alfvén speed differs in the differing flux tubes, a constant propagation speed of the interwoven structure may be difficult. A comparison of Figure 4b and 4d supports this conjecture. In Figure 7b the average angle between the flow and field for the 120-min subintervals of Figure 4 is plotted as a function of the value of $\sigma(\nu_A)/\langle \nu_A \rangle$ for each subinterval. The angle is smaller when $\sigma(\nu_A)/\langle \nu_A \rangle$ is smaller, that is, when the plasma is more homogeneous. The correlation between the angle and $\sigma(\nu_A)/\langle \nu_A \rangle$ is $R_{corr} = 0.78$, which is larger than it was for the Alfvénicity in Figure 7a.

In Figure 7c the Alfvénicity of each 120-min subinterval of Figure 4 is plotted as a function of the Alfvénspeed inhomogeneity $\sigma(v_A)/\langle v_A \rangle$ for each subinterval; a correlation coefficient of -0.55 is obtained with

BOROVSKY 7 of 14

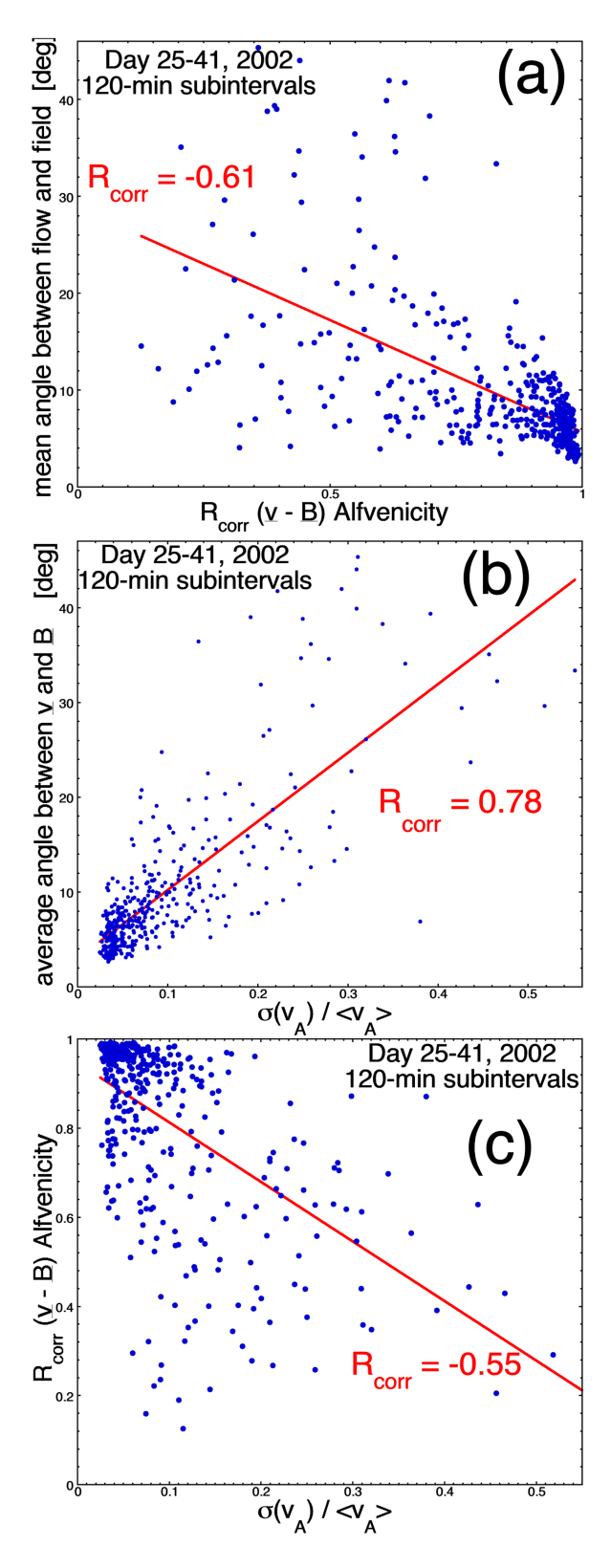


Figure 7. Connections between the mean angle (in the structure reference frame) between the flow and field, the Alfvénicity, and the Alfvén-speed inhomogeneity are explored in panels (a), (b), and (c). Each point represents an average value for a 120-min data subinterval from the entire 17-day D'Amicis et al. (2019) interval.

BOROVSKY 8 of 14

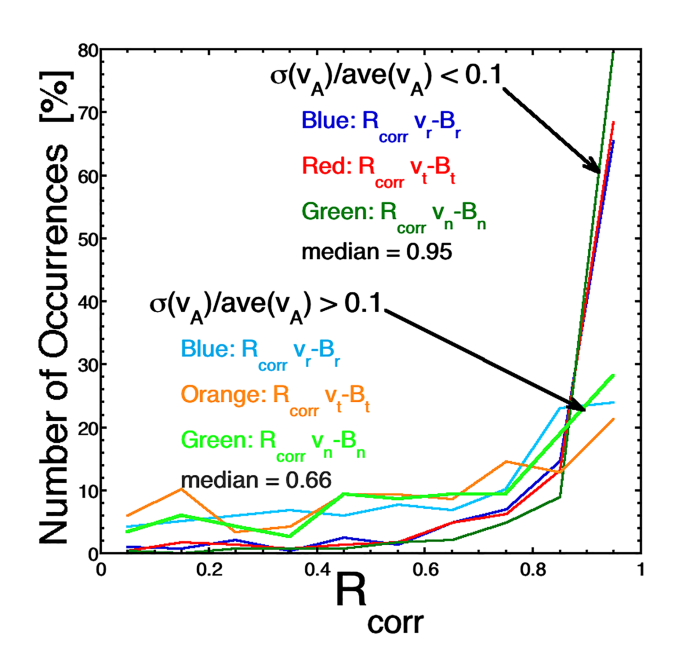


Figure 8. For highly homogeneous 120-min subintervals (upper labels) and for inhomogeneous 120-min subintervals (lower labels), the distribution of Alfvénicities is plotted for the 17-day D'Amicis et al. (2019) interval.

the Alfvénicity being higher when the plasma inhomogeneity is less. This is further explored in Figure 8 where the R-component (blue), Tcomponent (red), and N-component (green) correlations between v and B for the 120-min subintervals are binned separately for $\sigma (v_A)/\langle v_A \rangle <$ 0.1 and for $\sigma(v_A)/\langle v_A \rangle > 0.1$. The homogeneous $\sigma(v_A)/\langle v_A \rangle < 0.1$ distribution is dominated by high-Alfvénicity subintervals, with a median value of v-B correlation of 0.95, whereas the inhomogeneous $\sigma(v_A)/\langle v_A \rangle > 0.1$ distribution is dominated by weak-Alfvénicity subintervals with a median value of 0.66. Figures 7c and 8 imply that the inhomogeneity of the Alfvén speed in the solar wind plasma may be a controller of the Alfvénicity of the plasma. If so, the observed Alfvénicity of the solar wind may not be indicative of whether or not Alfvénic perturbations were injected at the Sun, but rather whether or not those Alfvén perturbations can survive in an inhomogeneous plasma. In magnetic flux tubes, kinklike Alfvénic perturbations propagate at a speed related to the Alfvén speed inside the flux tube (Edwin & Roberts, 1983; Ruderman & Roberts, 2006; Wilson, 1979). If the "flux tubes" of the heliospheric magnetic structure with differing Alfvén speeds are tangled, then the propagation of kink-type Alfvénic perturbations might not be possible; MHD modes in inhomogeneous plasma undergo complex changes (Belien et al., 1996; Lazzaro et al., 2000) including phase mixing (Soler & Terradas, 2015), dispersion (Lontano et al., 2000), and dissipation (Ryutova, 2015; Ryutova & Persson, 1984).

Similar arguments have been made for the control of the Alfvénicity of the solar wind plasma, but the discussion was based on "compressibility" rather than "inhomogeneity" (D'Amicis et al., 2016, 2019; D'Amicis & Bruno, 2015; Veltri et al., 1992). Compressibility in the solar wind literature is measured by variations in the plasma number density n or by variations in the magnetic field strength $B_{\rm mag}$. But variations in n in the solar wind are mostly owed to plasma "blocks" with differing number density (Borovsky, 2012b), manifested as jumps in the number density across current sheets in the magnetic structure. And variations in $B_{\rm mag}$ in the solar wind also show up as jumps in $B_{\rm mag}$ across current sheets (Barkhatov et al., 2003; Burlaga & Ness, 1969; Dalin et al., 2002; Franz et al., 2000), another form of plasma block structure. Additionally, magnetic holes (magnetic decreases) (Amariutei et al., 2011; Turner et al., 1977; Winterhalter et al., 2000) form another important source of changes in $B_{\rm mag}$. Rather than attributing the non-Alfvénicity of the solar wind to "compressibility" of the plasma, the discussion might be more insightful if the lack of Alfvénicity were attributed to plasma inhomogeneity or "lumpiness."

Along the lines of a discussion of compressibility in the solar wind, the solar wind has flows and flow shears at substantial Mach numbers, which under some circumstances might lead to compressive behavior. But when $\sigma(\nu_A)/\langle \nu_A \rangle$ is small, these flows are locally field aligned. One such shear can be seen in Figure 3a at time 33.80: A jump in the flow vector of 98 km/s in 3 s is seen. But it is a field-aligned flow, with a rotation of the flow vector being accompanied by a rotation of the magnetic-field vector; it is not the kind of high-Mach-number flow that would produce a change in $B_{\rm mag}$.

4.3. The Speed of the Magnetic Structure Through the Plasma

The speed of the motion of the magnetic structure through the proton plasma is explored in Figure 9. For the 2-hr subintervals of Days 25–41 of 2002 (cf. Figure 4) the velocity of the magnetic structure $\underline{v}_{structure}$ for each subinterval relative to the average of the measured solar wind velocity vector \underline{v}_{plasma} in each subinterval, normalized to the average Alfvén speed v_A for each subinterval, is plotted as a function of the inhomogeneity of the Alfvén speed in each subinterval (Figure 9a) and as a function of the \underline{v} - \underline{B} correlation (Alfvénicity) in each subinterval (Figure 9b). The vertical axis is the speed of the structure over the Alfvén speed in the reference frame of the solar wind plasma. Quality fits for $v_{structure}$ (wherein the angles between \underline{v} and \underline{B} are small in the moving reference frame of the structure) occur in Figure 9a for low values of $\sigma(v_A)/\langle v_A \rangle$ and quality fits for $\underline{v}_{structure}$ in Figure 9b occur for high values of R_{corr} . Note in both figures that for good fits the speed of the structure $|\underline{v}_{structure}|$ is rarely close to the Alfvén speed. In Figure 9c the normalized speed of the

BOROVSKY 9 of 14

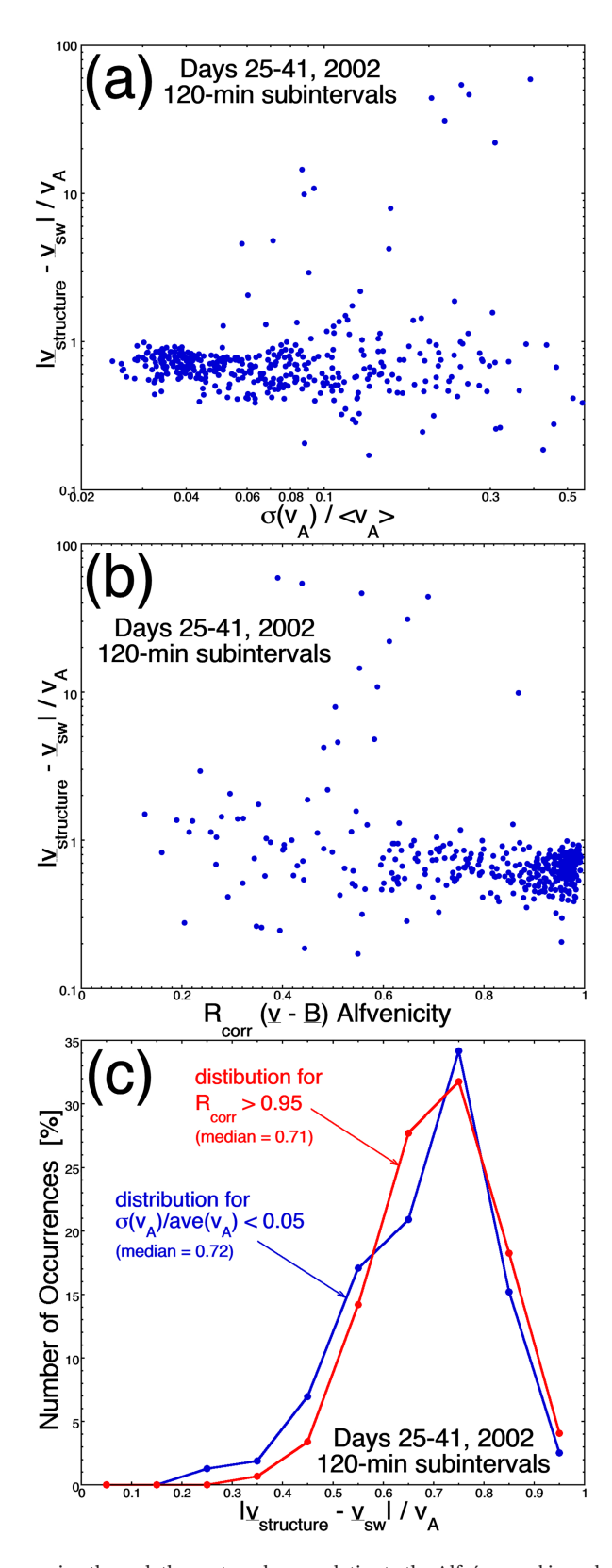


Figure 9. The speed of the magnetic structure moving through the proton plasma relative to the Alfvén speed is explored. In panel (a) the speed is plotted as a function of the Alfvén-speed inhomogeneity. In panel (b) the speed is plotted as a function of the Alfvénicity. Each point represents an average value for a 120-min data subinterval from the entire 17-day D'Amicis et al. (2019) interval. In panel (c) the distribution of speeds is plotted for the high-homogeneity subintervals (blue) and for the high-Alfvénicity subintervals.

BOROVSKY 10 of 14



magnetic structure relative to the plasma is binned for 2-hr subintervals wherein $\sigma(\nu_{\rm A})/\langle\nu_{\rm A}\rangle$ is less than 0.05 (blue curve) and for 2-hr intervals wherein $R_{\rm corr}$ is greater than 0.95 (red curve). Even for these cases where the plasma is homogeneous or the Alfvénicity is very high (or both), the structure speed is not at the Alfvén speed. As noted in the figure for the 2-hr subintervals, the median values of $|\underline{v}_{\rm structure} - \underline{v}_{\rm plasma}|$ are 0.72 $\nu_{\rm A}$ for the blue distribution and 0.71 $\nu_{\rm A}$ for the red distribution. For $\sigma(\nu_{\rm A})/\langle\nu_{\rm A}\rangle<0.05$ (blue) the mean value and standard deviation of $|\underline{v}_{\rm structure} - \underline{v}_{\rm plasma}|$ is 0.71 \pm 0.11 $\nu_{\rm A}$ and for the Alfvénicity $R_{\rm corr}(\underline{v}_{\rm -B})>0.95$ (red) the mean value and standard deviation of $|\underline{v}_{\rm structure} - \underline{v}_{\rm plasma}|$ is 0.68 \pm 0.14 $\nu_{\rm A}$. If the calculations of Figure 9 are repeated with shorter data subintervals (e.g., 30 min), the speed of the structure becomes, on average, closer to the Alfvén speed. A partial explanation of the reduction of the structure speed for a subinterval might be the angular spread $\Delta\theta$ in the magnetic field directions in the subinterval, which produces an angular spread in the vector Alfvén velocities $B/(4\pi\rho)^{1/2}$, resulting in a coherent structure speed that is related to $\nu_{\rm A}\cos(\Delta\theta)$.

4.4. Turbulence Scaling Estimates

For turbulence scaling estimates one might consider using the v_{\perp} values from the frame of motion of the heliospheric magnetic structure. For example, for the 2-hr coronal-hole-origin-plasma interval of Figure 3 the mean value of v_{\perp} is 5.2 km/s, whereas the value of $v_{\rm rms} = (\sigma (v_{\rm r})^2 + \sigma (v_{\rm t})^2 + \sigma (v_{\rm t})^2)^{1/2}$ is 30.6 km/s. Estimating the eddy turnover time (Bruno & Carbone, 2016; Tu & Marsch, 1995) $\tau_{\rm eddy} \sim L_{\perp}/v_{\perp}$ using $v_{\perp} = 5.2$ km/s yields an estimate of $\tau_{\rm eddy}$ that is ~6 times longer than the estimate using 30.6 km/s. (And the reader is reminded that this value of 5.2 km/s is undoubtedly an overestimate of v_{\perp} owing to the motion of the magnetic field direction during the 3-s measurement of the flow vector.) Hence, the age of the turbulence of the solar wind measured in turnover times may be much younger than existing estimates (e.g., Goldstein et al., 1995; Matthaeus et al., 1998; Roberts et al., 1992). In critical-balance calculations (Boldyrev, 2006; Goldreich & Sridhar, 1997; Podesta, 2010) the wavenumber ratio $k_{\parallel}/k_{\perp} = L_{\perp}/L_{\parallel} = v_{\perp}/v_{\rm A}$ will also come out smaller using v_{\perp} in the frame of the magnetic structure.

4.5. Propagating the Solar Wind to Earth

Knowledge about the movement of the heliospheric magnetic structure relative to the solar wind plasma can potentially lead to improvements in data-analysis schemes that advect upstream solar wind measurements to the Earth (Bargatze et al., 2005; Mailyan et al., 2008; Munteanu et al., 2013; Weimer et al., 2002, 2003; Weimer & King, 2008), critically used for magnetospheric physics and space weather. And note also that the velocity structure and plasma-properties structure of the heliosphere also moves with the magnetic structure. Those data-analysis schemes calculate the local orientation of structure at the upstream spacecraft and then advect the plane of the structure to the Earth at the measured vector velocity of the solar wind plasma. According to the present study, there is a correction to this advection velocity that can be determined using an interval of measurements to calculate the vector motion of the structure relative to the plasma.

The solar wind electric field is used for many studies of solar wind/magnetosphere coupling (e.g., Goertz et al., 1993; Milan et al., 2012; Reiff & Luhmann, 1986) (but see Borovsky & Birn, 2014, for a contrary view). That electric field in the reference frame of the earth is taken to be $\underline{E} = -(1/c)\underline{v}_{plasma} \times \underline{B}$, where \underline{v}_{plasma} is the vector velocity of the plasma as measured from the Earth's reference frame. In light of the knowledge that the magnetic structure of the solar wind moves relative to the plasma, it is worth reconsidering the calculation of the solar wind electric field E. To be specific, from a Maxwell's equations point of view there are two sources for the spatially dependent electric field associated with the moving magnetic structure (cf. Borovsky, 2016b): charge density $\rho_q = (1/c^2)\underline{v}_{plasma} \cdot j$ and time-dependent currents in the reference frame of the Earth $dj/dt = (v_{structure} \cdot \nabla)j$.

${\bf Acknowledgments}$

The author thanks Gian Luca Delzanno, Bob McPherron, Zdenek Nemecek, John Steinberg, Nicki Viall, and Dan Weimer for helpful conversations. This work was supported by the NASA Heliophysics Guest Investigator Program via Grant NNX17AB71G, by the NSF SHINE program via Award AGS-1723416, by the NASA Heliophysics LWS program via Grant NNX16AB75G, and by the NSF GEM Program. All WIND data sets utilized are available at the NASA Space Physics Data Facility (https://cdaweb.gsfc.nasa.gov).

References

Amariutei, O. A., Walker, S. N., & Zhang, T. L. (2011). Occurrence rate of magnetic holes between 0.72 and 1 AU: comparative study of Cluster and VEX data. *Annales Geophysicae*, 29(5), 717–722. https://doi.org/10.5194/angeo-29-717-2011

Bargatze, L. F., McPherron, R. L., Minamora, J., & Weimer, D. (2005). A new interpretation of Weimer et al.'s solar wind propagation delay technique. *Journal of Geophysical Research*, 110, A07105. https://doi.org/10.1029/2004JA010902

Barkhatov, N. A., Korolev, A. V., Zastenker, G. N., Ryazantseva, M. O., & Dalin, P. A. (2003). MHD simulations of the dynamics of sharp disturbances of the interplanetary medium and comparison with spacecraft observations. *Cosmic Research*, 41(6), 529–538. https://doi. org/10.1023/B:COSM.0000007951.49454.8a

Belien, A. J. C., Poedts, S., & Goedbloed, J. P. (1996). Magnetohydrodynamic continua and stratification induced Alfvén eigenmodes in coronal magnetic loops. *Physical Review Letters*, 76(4), 567–570. https://doi.org/10.1103/PhysRevLett.76.567

BOROVSKY 11 of 14

- Boldyrev, S. (2006). Spectrum of magnetohydrodynamic turbulence. *Physical Review Letters*, 96(11), 115002. https://doi.org/10.1103/ PhysRevLett.96.115002
- Borovsky, J. E. (2006). Eddy viscosity and flow properties of the solar wind: Co-rotating interaction regions, coronal-mass-ejection sheaths, and solar-wind/magnetosphere coupling. *Physics of Plasmas*, 13(5), 056505. https://doi.org/10.1063/1.2200308
- Borovsky, J. E. (2008). The flux-tube texture of the solar wind: Strands of the magnetic carpet at 1 AU? *Journal of Geophysical Research*, 113, A08110. https://doi.org/10.1029/2007JA012684
- Borovsky, J. E. (2012a). The effect of sudden wind shear on the Earth's magnetosphere: Statistics of wind-shear events and CCMC simulations of magnetotail disconnections. *Journal of Geophysical Research*, 117, A06224. https://doi.org/10.1029/2012JA017623
- Borovsky, J. E. (2012b). Looking for evidence of mixing in the solar wind from 0.31 to 0.98 AU. Journal of Geophysical Research, 117, A06107. https://doi.org/10.1029/2012JA017525
- Borovsky, J. E. (2016a). Plasma structure of the coronal-hole solar wind: Origins and evolution. *Journal of Geophysical Research: Space Physics*, 121, 5055–5087. https://doi.org/10.1002/2016JA022686
- Borovsky, J. E. (2016b). Relativity and the solar wind: The Maxwell-equation origins of the solar-wind motional electric field. *Journal of Electromagnetic Analysis and Applications*, 08(08), 133–151. https://doi.org/10.4236/jemaa.2016.88014
- Borovsky, J. E. (2018a). The spatial structure of the oncoming solar wind at Earth. *Journal of Atmospheric and Solar-Terrestrial Physics*, 177, 2–11. https://doi.org/10.1016/j.jastp.2017.03.014
- Borovsky, J. E. (2018b). Looking for evidence of wind-shear disconnections of the Earth's magnetotail: GEOTAIL measurements and LFM MHD simulations. *Journal of Geophysical Research: Space Physics*, 123, 5538, 5560. https://doi.org/10.1029/2018JA025456
- Borovsky, J. E. (2020). The magnetic structure of the solar wind: Ionic composition and the electron strahl. *Geophysical Research Letters*. 2019GL084586. https://doi.org/10.1029/2019GL084586
- Borovsky, J. E., & Birn, J. (2014). The solar-wind electric field does not control the dayside reconnection rate. *Journal of Geophysical Research: Space Physics*, 119, 751–760. https://doi.org/10.1002/2013JA019193
- Borovsky, J. E., Denton, M. H., & Smith, C. W. (2019). Some properties of the solar-wind turbulence at 1 AU statistically examined in the different types of solar-wind plasma. *Journal of Geophysical Research: Space Physics*, 124, 2406–2424. https://doi.org/10.1029/2019IA026580
- Bruno, R. (2019). Intermittency in solar wind turbulence from fluid to kinetic scales. Earth and Space Science, 6, 656.
- Bruno, R., & Carbone, V. (2016). Turbulence in the solar wind. Lecture Notes in Physics, 928, 1.
- Burlaga, L. F., & Ness, N. F. (1969). Tangential discontinuities in the solar wind. Solar Physics, 9(2), 467–477. https://doi.org/10.1007/BF02391672
- Chashei, I. V., & Shishov, V. I. (1995). Effects of turbulence on the propagation of interplanetary shock waves. *Astronomy Letters*, 21, 641. Dalin, P. A., Zastenker, G. N., Paularena, K. I., & Richardson, J. D. (2002). A survey of large, rapid solar wind dynamic pressure changes observed by Interball-1 and IMP 8. *Annales Geophysicae*, 20(3), 293–299. https://doi.org/10.5194/angeo-20-293-2002
- D'Amicis, R., & Bruno, R. (2015). On the origin of highly Alfvénic slow solar wind. The Astrophysical Journal, 805(1), 84. https://doi.org/10.1088/0004-637X/805/1/84
- D'Amicis, R., Bruno, R., & Matteini, L. (2016). Characterizing the Alfvénic slow wind: a case study. AIP Conference Proceedings, 1720,
- D'Amicis, R., Matteini, L., & Bruno, R. (2019). On the slow solar wind with high Alfvénicity: from composition and microphysics to spectral properties. *Monthly Notices of the Royal Astronomical Society*, 483, 4665.
- De Keyser, J., Roth, J. M., & Soding, A. (1998). Flow shear across solar wind discontinuities: WIND observations. *Geophysical Research Letters*, 25(14), 2649–2652. https://doi.org/10.1029/98GL51938
- Denskat, K. U., & Burlaga, L. F. (1977). Multispacecraft observations of microscale fluctuations in the solar wind. *Journal of Geophysical Research*, 82(19), 2693–2704. https://doi.org/10.1029/JA082i019p02693
- Edwin, P. M., & Roberts, B. (1983). Wave propagation in a magnetic cylinder. *Solar Physics*, 88, 179.
- Franz, M., Burgess, D., & Horbury, T. S. (2000). Magnetic field depressions in the solar wind. *Journal of Geophysical Research*, 105(A6), 12,725–12,732. https://doi.org/10.1029/2000JA900026
- Goertz, C. K., Shan, L.-H., & Smith, R. A. (1993). Prediction of geomagnetic activity. *Journal of Geophysical Research*, 98(A5), 7673–7684. https://doi.org/10.1029/92JA01193
- Goldreich, P., & Sridhar, S. (1997). Magnetohydrodynamic turbulence revisited. *Astrophysical Journal*, 485(2), 680–688. https://doi.org/10.1086/304442
- Goldstein, M. L., Roberts, D. A., & Matthaeus, W. H. (1995). Magnetohydrodynamic turbulence in the solar wind. Annual Review of Astronomy and Astrophysics, 33, 285.
- Guo, F., & Giacalone, J. (2010). The effect of large-scale magnetic turbulence on the acceleration of electrons by perpendicular collisionless shocks. *The Astrophysical Journal*, 715(1), 406–411. https://doi.org/10.1088/0004-637X/715/1/406
- Heinemann, M. A., & Siscoe, G. L. (1974). Shapes of strong shock fronts in an inhomogeneous solar wind. *Journal of Geophysical Research*, 79(10), 1349–1355. https://doi.org/10.1029/JA079i010p01349
- Kasper, J. C., Lazarus, A. J., Steinberg, J. T., Ogilvie, K. W., & Szabo, A. (2006). Physics-based tests to identify the accuracy of solar wind ion measurements: A case study with the Wind Faraday Cups. *Journal of Geophysical Research*, 111, A03105. https://doi.org/10.1029/ 2005JA011442
- Khabarova, O., & Zastenker, G. (2011). Sharp changes of solar wind ion flux and density within and outside current sheets. *Solar Physics*, 270(1), 311–329. https://doi.org/10.1007/s11207-011-9719-4
- Kocharov, L., Laitinen, T., & Vainio, R. (2013). The effect of turbulence intermittence on the emission of solar energetic particles by coronal and interplanetary shocks. *The Astrophysical Journal Letters*, 778(1), L5. https://doi.org/10.1088/2041-8205/778/1/L5
- Komar, C. M., Fermo, R. L., & Cassak, P. A. (2015). Comparative analysis of dayside magnetic reconnection models in global magneto-sphere simulations. *Journal of Geophysical Research: Space Physics*, 120, 276–294. https://doi.org/10.1002/2014JA020587
- Lavraud, B., Ruffenach, A., Rouillard, A. P., Kajdic, P., Manchester, W. B., & Lugaz, N. (2014). Geo-effectiveness and radial dependence of magnetic cloud erosion by magnetic reconnection. *Journal of Geophysical Research: Space Physics*, 119, 26–35. https://doi.org/10.1002/ 201314.019154
- Lazzaro, E., Lontano, M., & Ryutov, D. D. (2000). Linear magnetohydrodynamic waves in a finely stratified plasma. *Physical Review E*, 61(3), 3069–3077. https://doi.org/10.1103/PhysRevE.61.3069
- Lepping, R. P., Acuna, M. H., Burlaga, L. F., Farrell, W. M., Slavin, J. A., Schatten, K. H., et al. (1995). The WIND Magnetic Field Investigation. Space Science Reviews, 71(1-4), 207–229. https://doi.org/10.1007/BF00751330
- Li, G., & Qin, G. (2011). A solar wind model with current sheets. ASP Conference Series, 444, 117.

BOROVSKY 12 of 14

- Lin, R. P., Anderson, K. A., Ashford, S., Carlson, C., Curtis, D., Ergun, R., et al. (1995). A three-dimensional plasma and energetic particle investigation for the WIND spacecraft. Space Science Reviews, 71(1-4), 125–153. https://doi.org/10.1007/BF00751328
- Liu, Y.-H., Hesse, M., & Kuznetsova, M. (2015). Orientation of X lines in asymmetric magnetic reconnection—Mass ratio dependency. Journal of Geophysical Research: Space Physics, 120, 7331–7341. https://doi.org/10.1002/2015JA021324
- Lontano, M., Lazzaro, E., & Ryutov, D. (2000). Dispersion of long MHD waves in a finely structured plasma. *Physica Scripta*, *T84*(1), 52. https://doi.org/10.1238/Physica.Topical.084a00052
- Mailyan, B., Munteanu, C., & Haaland, S. (2008). What is the best method to calculate the solar wind propagation delay? *Annales Geophysicae*, 26(8), 2383–2394. https://doi.org/10.5194/angeo-26-2383-2008
- Mariani, F., Bavassano, B., & Villante, U. (1983). A statistical study of MHD discontinuities in the inner solar system: Helios 1 and 2. Solar Phyics, 83(2), 349–365. https://doi.org/10.1007/BF00148285
- Matthaeus, W. H., Smith, C. W., & Oughton, S. (1998). Dynamical age of solar wind turbulence in the outer heliosphere. *Journal of Geophysical Research*, 103(A4), 6495–6502. https://doi.org/10.1029/97JA03729
- McCracken, K. G., & Ness, N. F. (1966). The collimation of cosmic rays by the interplanetary magnetic field. *Journal of Geophysical Research*, 71(13), 3315–3318. https://doi.org/10.1029/JZ071i013p03315
- Milan, S. E., Gosling, J. S., & Hubert, B. (2012). Relationship between interplanetary parameters and the magnetopause reconnection rate quantified from observations of the expanding polar cap. *Journal of Geophysical Research*, 117, A03226. https://doi.org/10.1029/2011JA017082
- Morley, S. K., Welling, D. T., & Woodroffe, J. R. (2018). Perturbed input ensemble modeling with the Space Weather Modeling Framework. Space Weather, 16, 1330–1347. https://doi.org/10.1029/2018SW002000
- Munteanu, C., Haaland, S., Mailyan, B., Echim, M., & Mursula, K. (2013). Propagation delay of solar wind discontinuities: Comparing different methods and evaluating the effect of wavelet denoising. *Journal of Geophysical Research: Space Physics*, 118, 3985–3994. https://doi.org/10.1002/jgra.50429
- Nemecek, Z., Durovcova, T., Safrankova, J., Nemec, F., Matteini, L., Stansby, D., et al. (2020). What is the solar wind frame of reference? The Astrophysical Journal. AAS19472R2 in press
- Neugebauer, M. (1985). Alignment of velocity and field changes across tangential discontinuities in the solar wind. *Journal of Geophysical Research*, 90(A7), 6627. https://doi.org/10.1029/JA090iA07p06627
- Neugebauer, M., & Giacalone, J. (2010). Progress in the study of interplanetary discontinuities. AIP Conference Proceedings, 1216, 194. Neugebauer, M., & Giacalone, J. (2015). Energetic particles, tangential discontinuities, and solar flux tubes. *Journal of Geophysical Research: Space Physics*, 120, 8281–8287. https://doi.org/10.1002/2015JA021632
- Niemiec, J., & Ostrowski, M. (2004). Cosmic-ray acceleration at relativistic shock waves with a "realistic" magnetic field structure. The Astrophysical Journal, 610(2), 851–867. https://doi.org/10.1086/421730
- Owens, M. J., Wicks, R. T., & Horbury, T. S. (2011). Magnetic discontinuities in the near-Earth solar wind: Evidence of in-transit turbulence or remnants of coronal structure? *Solar Physics*, 269(2), 411–420. https://doi.org/10.1007/s11207-010-9695-0
- Podesta, J. J. (2010). Theory of solar wind turbulence with scale-dependent alignment, anisotropy, and cross-helicity. AIP Conference Series, 1216, 115.
- Qin, G., & Li, G. (2008). Effect of flux tubes in the solar wind on the diffusion of energetic particles. *The Astrophysical Journal*, 682(2), L129–L132. https://doi.org/10.1086/591229
- Reiff, P. H., & Luhmann, J. G. (1986). Solar wind control of the polar-cap voltage. In Y. Kamide, & J. A. Slavin (Eds.), Solar wind-magnetosphere coupling, (pp. 453–476). Tokyo: Terra Scientific.
- Riazantseva, M. O., Khabarova, O. V., Zastenker, G. N., & Richardson, J. D. (2005). Sharp boundaries of solar wind plasma structures and an analysis of their pressure balance. *Cosmic Research*, 43(3), 157–164. https://doi.org/10.1007/s10604-005-0030-8
- Roberts, D. A., Goldstein, M. L., Matthaeus, W. H., & Ghosh, S. (1992). Velocity shear generation of solar wind turbulence. *Journal of Geophysical Research*, 97(A11), 17,115. https://doi.org/10.1029/92JA01144
- Ruderman, M., & Roberts, B. (2006). Leaky and non-leaky kink oscillations of magnetic flux tubes. *Journal of Plasma Physics*, 72(03), 285. https://doi.org/10.1017/S0022377805004101
- Ryutova, M. (2015). Physics of magnetic flux tubes. Berlin: Springer-Verlag.
- Ryutova, M., & Persson, M. (1984). Dispersion properties and enhanced dissipation of MHD-oscillations in a plasma with random inhomogeneities. *Physica Scripta*, 29(4), 353–359. https://doi.org/10.1088/0031-8949/29/4/013
- Sandroos, A., & Vainio, R. (2006). Particle acceleration at shocks propagating in inhomogeneous magnetic fields. *Astronomy & Astrophysics*, 455(2), 685–695. https://doi.org/10.1051/0004-6361:20054754
- Schwenn, R. (2000). Heliospheric 3D structure and CME propagation as seen from SOHO: Recent lessons for space weather predictions. $Advances\ in\ Space\ Research,\ 26(1),\ 43-53.\ https://doi.org/10.1016/S0273-1177(99)01025-X$
- Siscoe, G. L., Davis, L., Coleman, P. J., Smith, E. J., & Jones, D. E. (1968). Power spectra and discontinuities of the interplanetary magnetic field: Mariner 4. *Journal of Geophysical Research*, 73(1), 61–82. https://doi.org/10.1029/JA073i001p00061
- Soler, R., & Terradas, J. (2015). Magnetohydrodynamic waves in nonuniform solar flux tubes: Phase mixing and energy cascade to small scales. *The Astrophysical Journal*, 803(1), 43. https://doi.org/10.1088/0004-637X/803/1/43
- Sonnerup, B. U. O. (1974). Magnetopause reconnection rate. Journal of Geophysical Research, 79(10), 1546–1549. https://doi.org/10.1029/ JA079i010v01546
- Tessein, J. A., Ruffolo, D., Matthaeus, W. H., & Wan, M. (2016). Local modulation and trapping of energetic particles by coherent magnetic structures. *Geophysical Research Letters*, 43, 3620–3627. https://doi.org/10.1002/2016GL068045
- Trenchi, L., Bruno, R., Telloni, D., D'Amicis, R., Marcucci, M. F., Zurbuchen, T. H., & Weberg, M. (2013). Solar energetic particle modulation associated with coherent magnetic structures. *The Astrophysical Journal*, 770(1), 11. https://doi.org/10.1088/0004-637X/770/1/11 Tu, C.-Y., & Marsch, E. (1995). MHD structures, waves and turbulence in the solar wind. *Space Science Reviews*, 73(1-2), 1–210. https://doi.
- org/10.1007/BF00748891

 Tu, C.-Y., Wang, X., He, J., Marsch, E., & Wang, L. (2016). Two cases of convecting structure in the slow solar wind turbulence. AIP
- Conference Proceedings, 1720, 040017.
 Turner, J. M., Burlaga, L. F., Ness, N. F., & Lemaire, J. F. (1977). Magnetic holes in the solar wind. *Journal of Geophysical Research*, 82(13),
- 1921–1924. https://doi.org/10.1029/JA082i013p01921 van der Holst, B., Poedts, S., Chane, E., Jacobs, C., Dubey, G., & Kimpe, D. (2005). Modelling of solar wind, CME initiation and CME
- propagation. Space Science Reviews, 121(1-4), 91–104. https://doi.org/10.1007/s11214-006-6541-7

 Veltri, P., Malara, F., & Primavera, L. (1992). Correlation, anisotropy and compressibility of low frequency fluctuations in solar wind. In Solar Wind Seven, (p. 559). Oxford: Pergammon.

BOROVSKY 13 of 14



- Veltri, P., & Mangeney, A. (1999). Scaling laws and intermittent structures in solar wind MHD turbulence. AIP Conference Proceedings, 471, 543.
- Walsh, B. M., Bhakyaibul, T., & Zou, Y. (2019). Quantifying the uncertainty of using solar wind measurements for geospace inputs. Journal of Geophysical Research: Space Physics, 124, 3291–3302. https://doi.org/10.1029/2019JA026507
- Weimer, D. R., & King, J. H. (2008). Improved calculations of IMF phase-front angles and propagation time delays. *Journal of Geophysical Research*, 113, A01105. https://doi.org/10.1029/2007JA012452
- Weimer, D. R., Ober, D. M., Maynard, N. C., Collier, M. R., McComas, D. J., Ness, N. F., et al. (2003). Predicting IMF propagation delay times using the minimum variance technique. *Journal of Geophysical Research*, 108(A1), 1026. https://doi.org/10.1029/2002JA009405
- Weimer, D. R., Ober, D. M., NMaynard, N. C., Burke, W. J., Collier, M. R., McComas, D. J., et al. (2002). Variable time delays in the propagation of the interplanetary magnetic field. *Journal of Geophysical Research*, 107(A8), 1210. https://doi.org/10.1029/2001JA009102
- Wilson, P. R. (1979). Hydromagnetic wave modes in magnetic flux tubes. Astronomy & Astrophysics, 71, 9.
- Winterhalter, D., Smith, E. J., Neugebauer, M., Goldstein, B. E., & Tsurutani, B. T. (2000). The latitudinal distribution of solar wind magnetic holes. *Geophysical Research Letters*, 27(11), 1615–1618. https://doi.org/10.1029/1999GL003717
- Xu, F., & Borovsky, J. E. (2015). A new 4-plasma categorization scheme for the solar wind. *Journal of Geophysical Research: Space Physics*, 120, 70–100. https://doi.org/10.1002/2014JA020412
- Zank, G. P., Zhou, Y., Matthaeus, W. H., & Rice, W. K. M. (2003). The interaction of turbulence with shock waves. AIP Conference Proceedings, 679, 417.
- Zhou, Y., & Feng, X. (2017). Numerical study of the propagation characteristics of coronal mass ejections in a structured ambient solar wind. Journal of Geophysical Research: Space Physics, 122, 1451–1462. https://doi.org/10.1002/2016JA023053
- Zimbardo, G., Pommois, P., & Veltri, P. (2008). Visualizing particle transport across magnetic flux tubes in anisotropic magnetic turbulence. *IEEE Transactions on Plasma Science*, 36(4), 1114–1115. https://doi.org/10.1109/TPS.2004.924572

BOROVSKY 14 of 14